Eur. Phys. J. D **30**, 209–215 (2004)
DOI: 10.1140/epjd/e2004-00074-6

THE EUROPEAN PHYSICAL JOURNAL D

Three-dimensional vibronic analysis of the B′ system of Na_3

I. Bâldea[a] and H. Köppel[b]

Theoretische Chemie, Physikalisch-Chemisches Institut, Universität Heidelberg, Im Neuenheimer Feld 229, 69120 Heidelberg, Germany

Received 9 March 2004
Published online 26 May 2004 –

Abstract. The vibronic structure of the B′ system in the two-photon ionization spectrum of Na_3 is investigated theoretically, based on an earlier coupling scheme with three interacting potential energy surfaces (pseudo Jahn-Teller coupling). This is extended in the present work to allow for additional ab initio data in the modeling, to include the totally symmetric vibrational mode and to treat a higher excited state in the electronic manifold. Important features of the experimental recording can thus be reproduced, although some unsatisfactory aspects remain. The implications for the nonadiabatic nature of the underlying nuclear motion, as well as directions for future work, are discussed.

PACS. 36.40.-c Atomic and molecular clusters – 36.20.Ng Vibrational and rotational structure, infrared and Raman spectra – 36.40.Mr Spectroscopy and geometrical structure of clusters

1 Introduction

The sodium trimer, Na_3, has received continuous attention in the literature as a representative example of a small metal atom cluster, and because of its unusual and interesting spectroscopic and dynamical properties (see, for example, references [1–16] and references cited therein). In its electronic ground state it is a Jahn-Teller (JT) distorted equilateral triangle with three equivalent (obtuse-angled) $^2B_2$ minima and three (acute-angled) $^2A_1$ saddle points [1,2,4]. Similar effects are operative also in excited electronic states, leading to fluxional nuclear motion and geometric phase effects for the so-called pseudo-rotation (see, for example, references [3–6,9–14,16]). These have their origin in specific properties of the potential energy surfaces and have been investigated extensively in the experimental and theoretical work mentioned above.

An intriguing aspect emerging from this work is the possibility of multi-state vibronic interactions, involving more than two coupled potential energy surfaces. It has been previously shown that the electronic B state of Na_3 can be successfully described theoretically within the so-called pseudo-Jahn-Teller (PJT)-model, based on an interaction of a doubly degenerate electronic E state with a close-lying electronic A state [4,6,17–19]. A variety of experimental findings on the B system, including femtosecond time-resolved spectroscopy, have been correctly reproduced by the theoretical approach [6,17–19], in spite of certain simplifications: the number of independent model parameters has been reduced as much as possible and the totally symmetric (stretching, or breathing) vibrational coordinate has been ignored.

According to the PJT approach the B state is the lowest of three coupled states (two being degenerate at the D_{3h} conformation), for which the nonadiabatic coupling effects are weak. The situation becomes more complex, and also interesting, for transitions to higher states of this coupled manifold for which strong nonadiabatic coupling effects are expected. A typical candidate for such a state is the so-called B′ state with an excitation wavelength of ∼560 nm [20,21]. It has been characterized in some detail experimentally [21] and occurs at the expected energy (see also below), with a degree of complexity as is typical for such a situation.

In the present paper we aim to describe the two-photon ionization (TPI) spectrum of the B′ excited state of the Na_3 molecule using the same conceptual approach as in our earlier work on the B state [6,17]. In the first stage of the investigation, we have employed the same Hamiltonian and parameter values used previously [6,17]. However, it turned out that the TPI spectrum of the B′ system obtained in this way considerably differs from the experimental one [21]. In order to improve the agreement between theory and experiment, we progressively extended the model Hamiltonian of references [6,17] to account for the available ab initio data for Na_3 [4,22,23] and also included the totally-symmetric vibrational mode. The approach is briefly described below, followed by a discussion of the results achieved and, finally, of directions for future work.

[a] *Permanent address*: National Institute for Lasers, Plasmas and Radiation Physics, ISS, 76900 Bucharest-Măgurele, Romania. e-mail: ioan@pci.uni-heidelberg.de
[b] e-mail: a86@ix.urz.uni-heidelberg.de

2 Theoretical considerations

As is well-known, the vibrational motion of the Na_3 cluster can be described by three normal modes, which are expressed in terms of the Cartesian coordinates $x_{1,2,3}$ and $y_{1,2,3}$ of the three atoms as follows [24]:

$$\begin{aligned} q_s &= (-x_1 + x_2/2 - y_2\sqrt{3/2} + x_3/2 + y_3\sqrt{3/2})/\sqrt{3}, \\ q_x &= (y_1 + x_2\sqrt{3/2} - y_2/2 - x_3\sqrt{3/2} - y_3/2)/\sqrt{3}, \\ q_y &= (+x_1 - x_2/2 - y_2\sqrt{3/2} - x_3/2 + y_3\sqrt{3/2})/\sqrt{3}. \end{aligned} \quad (1)$$

$q_{s,x,y}$ describe the symmetric stretching (or breathing, or totally symmetric), asymmetric stretching and bending modes, respectively, where the latter two combine to yield the doubly degenerate mode at the D_{3h} conformation. The corresponding dimensionless coordinates will be denoted by $Q_{s,x,y}$, respectively.

To describe the B′ state of Na_3, we shall adopt, as usual, a diabatic basis for the electronic states which depends only weakly on the nuclear coordinates. Neglecting this weak dependence the kinetic energy part of the Hamiltonian matrix becomes diagonal. The vibronic coupling of the electronic states is taken into account by expanding the off-diagonal terms of the potential energy matrix up to the second order [6,17] in the nuclear displacements from the D_{3h} conformation. By choosing D_{3h} as reference geometry, the Hamiltonians $\mathbf{H}_X$ for the ground state and $\mathbf{H}_e$ for the excited state manifold take the following forms:

$$\begin{aligned} \mathbf{H}_X = &\left[\hat{T}_N^X + \frac{\omega^X}{2}\rho^2 + \frac{\omega_s^X}{2}\left(Q_s - \tilde{Q}_s\right)^2\right] \\ &\times \left(|\Psi_+\rangle\langle\Psi_+| + |\Psi_-\rangle\langle\Psi_-|\right) \\ &+ \left[|\Psi_+\rangle\left(k_X\rho e^{-i\phi} + \frac{g_X}{2}\rho^2 e^{2i\phi}\right)\langle\Psi_-| + \text{h.c.}\right], \end{aligned} \quad (2)$$

$$\begin{aligned} \mathbf{H}_e = &\left[\hat{T}_N^E + \epsilon^E + \frac{\omega^E}{2}\rho^2 + \frac{\omega_s^E}{2}\left(Q_s - \tilde{Q}_s\right)^2 - K_E Q_s\right] \\ &\times \left(|\Phi_+\rangle\langle\Phi_+| + |\Phi_-\rangle\langle\Phi_-|\right) \\ &+ \left[\hat{T}_N^A + \epsilon^A + \frac{\omega^A}{2}\rho^2 + \frac{\omega_s^A}{2}\left(Q_s - \tilde{Q}_s\right)^2 - K_A Q_s\right] \\ &\times |\Phi_A\rangle\langle\Phi_A| + \left[|\Phi_A\rangle\left(\lambda\rho e^{i\phi} + \frac{f}{2}\rho^2 e^{-2i\phi}\right)\langle\Phi_-|\right. \\ &+ |\Phi_A\rangle\left(\lambda\rho e^{-i\phi} + \frac{f}{2}\rho^2 e^{2i\phi}\right)\langle\Phi_+| \\ &\left.+ |\Phi_+\rangle\left(k\rho e^{-i\phi} + \frac{g}{2}\rho^2 e^{2i\phi}\right)\langle\Phi_-| + \text{h.c.}\right]. \end{aligned} \quad (3)$$

In the r.h.s. of these equations the indices X, E, and A denote the electronic state in question. The polar coordinates ρ and ϕ for the latter are related to the dimensionless normal coordinates Q_x and Q_y by $\rho e^{i\phi} = Q_y + iQ_x$. The $\hat{T}_N$'s denote the corresponding kinetic energy operators, e.g.: $2\hat{T}_N^X = -\omega^X(\partial^2/\partial Q_x^2 + \partial^2/\partial Q_y^2) - \omega_s^X\partial^2/\partial Q_s^2$. In the calculations, we have always used $\omega_s^E = \omega_s^A$.

The interaction of the molecule with the radiation field will be treated within the dipole approximation, which is fully justified for weak field strengths. The expression of the dipole operator $\vec{\mathbf{D}}$ follows from the requirement that $\vec{\mathbf{D}}$ forms the basis of an E′ irreducible representation of D_{3h} [6,18,19]:

$$\begin{aligned} \vec{\mathbf{D}} = &|\Phi_-\rangle\vec{\mu}_+^{EE}\langle\Psi_+| + |\Phi_+\rangle\vec{\mu}_-^{EE}\langle\Psi_-| \\ &+ |\Phi_A\rangle\vec{\mu}_-^{EA}\langle\Psi_+| - |\Phi_A\rangle\vec{\mu}_+^{EA}\langle\Psi_-|, \end{aligned} \quad (4)$$

where $\vec{\mu}_\pm^{EE}$ couples the ground and excited E states, $\vec{\mu}_\pm^{EA}$ the ground state E with the excited A state ($\vec{\mu}_\pm^e = \vec{\mu}_y^e \pm i\vec{\mu}_x^e; e = EE, EA$). The transition dipole elements in the *diabatic* basis are assumed independent of nuclear coordinates (generalized Condon approximation). Lacking further information about the μ's, we assume them to be real constants with the same magnitude.

The TPI spectrum is determined by the transition probability for the electronic excitation $Na_3(X) \rightarrow Na_3(B')$ (first photon) and for ionization $Na_3(B') \rightarrow Na_3^+$ (second photon). The latter is expected to depend smoothly on the excitation energy. Since only a qualitative rather than quantitative comparison of the theory with experiment is possible at present, we shall simply disregard the second photon and approximate the TPI intensities by those of the first (dipole) transition. To compute this by means of the golden rule, one needs the initial vibronic state before excitation. For this, even at very low temperatures, one has to consider both the vibronic ground state and the next one (a tunnel partner), because the (tunneling) splitting between them is extremely small [17]. For symmetry reasons, the total spectrum is a superposition of three independent spectra, similar to the case of the B system [17].

In the actual calculations, we have not used the three lowest, almost degenerate vibronic eigenstates of $\mathbf{H}_X$ from equation (2). Instead, we have approximated the initial vibronic state by the product of Gaussian wave packets corresponding to the three modes:

$$\exp\left[-\frac{(Q_x - \tilde{Q}_x)^2}{2\sigma_x^2} - \frac{(Q_y - \tilde{Q}_y)^2}{2\sigma_y^2} - \frac{(Q_s - \tilde{Q}_s)^2}{2\sigma_s^2}\right]. \quad (5)$$

This initial wave packet has been localized at one of the three classically equivalent minima of the electronic ground state, in agreement with available ab initio and experimental results. Based on ab initio studies [4,22] and previous investigations of the B system [6,19], we set $\tilde{Q}_y = 6.859$ (corresponding to $\tilde{X}_y = 0.737$ Å), $\tilde{Q}_x = 0$ ($\tilde{X}_x = 0$), $\sigma_y = 1.2083$, and $\sigma_x = 1.5648$. Within the approach based on the initial wave packet (5), out of the model parameters entering equation (2), we only need the frequency ω_s^X of the symmetric mode in the ground electronic state, since it determines the width parameter σ_s according to:

$$\sigma_s = \sqrt{\omega_s^E/\omega_s^X}. \quad (6)$$

In accord with the experimental [21] and ab initio [4] data, we have employed a value of $\omega_s^X = 140$ cm^{-1}. For reasons exposed below, the packet center has been placed at a

Table 1. Values of the model parameters used in the various stages of the present investigation. These values have been deduced from references [4,22] in the manner described in the text.

Parameter	a	b	c	d	e	f	g	h
ω^A (cm^{-1})	127	127	127	127	127	127	127	127
ω^E (cm^{-1})	127	127	62	62	62	62	62	62
$\epsilon^E - \epsilon^A$ (cm^{-1})	0	0	275	275	275	275	275	275
λ/ω^A	3.07	3.07	1.85	1.85	1.85	1.85	1.85	1.85
$f/\omega^A \times 10^3$	4.5	4.5	4.5	4.5	4.5	4.5	4.5	4.5
k/ω^A	0	0	0	0	0.356	−0.356	0.356	−0.356
$g/\omega^A \times 10^3$	0	0	0	0	0.865	0.865	0.865	0.865
ω_s^X (cm^{-1})	-	140	-	140	-	-	140	140
$\omega_s^E = \omega_s^A$ (cm^{-1})	-	127	-	105	-	-	105	105
K_E/ω_s^E	-	2.304	-	2.304	-	-	2.304	2.304
K_A/ω_s^A	-	0.780	-	0.780	-	-	0.780	0.780

value $\tilde{Q}_s$ of the dimensionless coordinate corresponding to $\tilde{X}_s = 3.70$ Å.

In the course of the investigations, we have varied systematically the frequencies and the coupling strengths in order to reproduce features of experimental spectra. For each set of parameters, we have adjusted the zero of energy (by setting the value $\bar{\epsilon} = (\epsilon^E + \epsilon^A)/2$ appropriately) to reproduce the onset (≃625 nm) of the experimental B spectrum [20].

Let us now consider the excited electronic states in more detail. In C_{2v} symmetry ($\phi = \pi$, $\rho = -Q_y$), the adiabatic potential energies corresponding to equation (3) can be expressed as:

$$\begin{aligned} V_0(Q_y,Q_s) &= V_E(Q_y,Q_s) - V_{JT}(Q_y), \\ V_\pm(Q_y,Q_s) &= \frac{1}{2}\left[V_E(Q_y,Q_s) + V_A(Q_y,Q_s) + V_{JT}(Q_y)\right] \\ &\pm \left(\frac{1}{4}\left[V_E(Q_y,Q_s) - V_A(Q_y,Q_s)\right.\right. \\ &\left.\left. + V_{JT}(Q_y)\right]^2 + 2V_{PJT}^2(Q_y)\right)^{\frac{1}{2}}, \end{aligned} \tag{7}$$

where:

$$\begin{aligned} V_{E,A}(Q_y,Q_s) &\equiv \epsilon^{E,A} + \frac{1}{2}\omega^{E,A}Q_y^2 + \frac{1}{2}\omega_s^E\left(Q_s - \tilde{Q}_s\right)^2 \\ &\quad - K_{E,A}\left(Q_s - \tilde{Q}_s\right), \\ V_{PJT}(Q_y) &\equiv -\lambda Q_y + \frac{1}{2}fQ_y^2, \\ V_{JT}(Q_y) &\equiv -kQ_y + \frac{1}{2}gQ_y^2. \end{aligned} \tag{8}$$

Within the present approach, the three adiabatic curves $V_{0,\pm}$ of equation (7) will be employed to describe the B system and the B′ system of Na_3. The lower curve (V_-) corresponds to the final state of the B system (the $4\,^2A_1$ state in the ab initio study of Ref. [4]), while the middle (V_0) and the upper (V_+) curves (degenerate at the D_{3h} conformation $Q_y = 0$, cf. Eqs. (7, 8)) should model the B′ system, more precisely the $3\,^2B_2$ and $5\,^2A_1$ curves of reference [4], respectively. To this aim, the ab initio curves $4\,^2A_1$, $3\,^2B_2$ and $5\,^2A_1$ [4] (represented by solid lines in Fig. 1) should be fitted by V_-, V_0, and V_+, respectively, to determine the model parameters entering equations (7, 8).

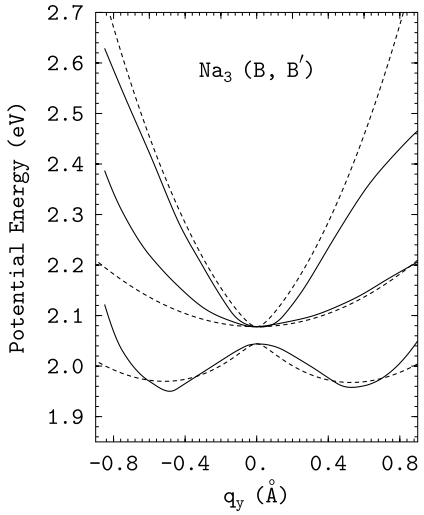

Fig. 1. Adiabatic potential energy curves computed ab initio by Cocchini et al. [4] (solid lines) and fitted analytically (dashed lines) by using $\omega^A = 127\,cm^{-1}$, $\omega^E = 62$ cm^{-1}, $\lambda/\omega^A = +1.85$, $f/\omega^A = 0.0045$, $E_E - E_A = 275$ cm^{-1} in equations (7, 8). The solid lines correspond to the states $4\,^2A_1$, $3\,^2B_2$ and $5\,^2A_1$ of reference [4], the dashed lines correspond to V_-, V_0, and V_+ (energies in increasing order in both cases). The value of the bending coordinate at the ground state minimum is $q_y = +0.737$ Å.

In references [6,17] the attention has been focused on the B system within a two-dimensional (2D) approach where the stretching mode (Q_s) has been ignored. Equations (3, 8) reduce to the 2D case of references [6,17] if the constraints used there are imposed: $\epsilon^E = \epsilon^A$, $\omega^E = \omega^A$, and $k = g = 0$. With these constraints and by optimizing for the B system one obtains [6] a set of parameter values (parameter set a in Tab. 1), yielding a TPI spectrum of the B′ system at variance with the experimental one; compare Figures 2 and 3a. Therefore, in order to improve the agreement between theory and experiment,

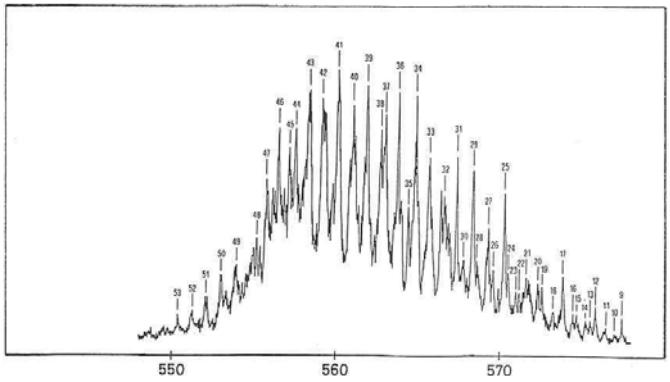

Fig. 2. Experimental B′ system in the two-photon ionization spectrum of Na_3.

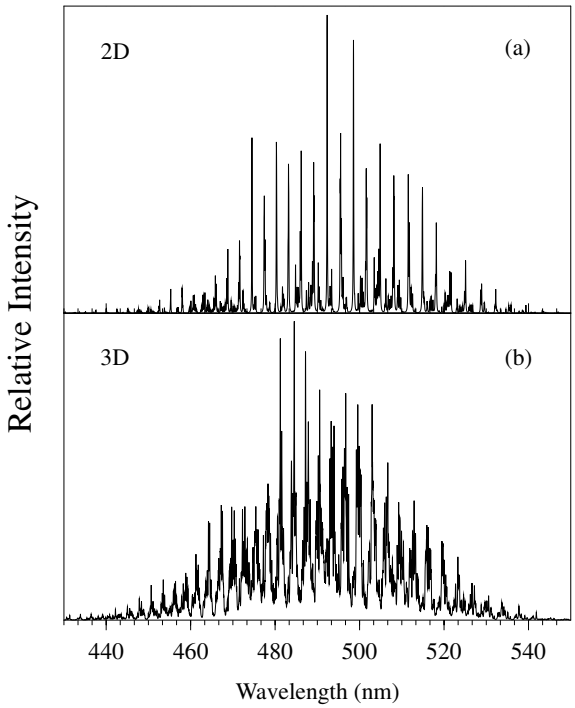

Fig. 3. Spectrum obtained by means of: (a) two-dimensional calculations using parameter set a, and (b) three-dimensional calculations using parameter set b. (For the parameter values, see Tab. 1.)

we have progressively modified the parameter values used in references [6,17] to account for information provided by available ab initio studies. This will be discussed in detail in Section 3.

In all the cases presented in this paper, the line spectra obtained by exact numerical diagonalization have been convoluted by using a Lorentzian function of halfwidth $\Gamma = 0.25\,\text{meV}$. For the subsequent considerations, it is worth noting that the B′ system of Na_3 is determined by the transitions from the ground state to the lower curve (V_0) of the degenerate, or E, state of the present electronic manifold; this is located in the middle of Figures 1 and 5.

3 Results and discussion

In an attempt to obtain theoretical spectra which are in better agreement with the experimental spectrum (Fig. 2) than that of Figure 3a, we have included the stretching mode (Q_s) in the calculations. In addition, we have reconsidered the parameter values used earlier [6,17].

To estimate the parameters characterizing the stretching mode, we have used the Q_s-dependent curves computed ab initio [4]. The two Q_s-dependent curves for the states $4^2A_1(\equiv 2^2A_1'$ at $D_{3h})$ and $5^2A_1 \equiv 3^2B_2$ $(\equiv 3^2E'$ at $D_{3h})$ computed ab initio at $Q_x = Q_y = 0$ (Figs. 6a and 6b in Ref. [4]) can be well fitted around their minimum (located at $q_s \approx 3.83$ Å and $q_s \approx 4.03$ Å, respectively), by using a common value $\omega_s^E = \omega_s^A = 105\ \text{cm}^{-1}$ in the formulae (7) for $V_-(Q_y = 0, Q_s)$ and $V_0(Q_y = 0, Q_s) \equiv V_+(Q_y = 0, Q_s)$, respectively. The values of K_A and K_E could be determined from the shift of the minima of these states along the Q_s-axis with respect to the ground state minimum (located at $q_s \approx 3.50$ Å). This procedure yields $K_E/\omega_s^E \approx 5.00$ and $K_A/\omega_s^A \approx 3.80$. These values are unusually large, but, as we immediately argue, this estimate is unrealistic. The reason is that, while the ground state minimum at $Q_{x,y} = 0$ is located at $q_s \approx 3.50$ Å, the *absolute*, JT-distorted minimum extracted from Figure 5a of reference [4] is at $\tilde{X}_s \approx 3.70$ Å. Therefore, one should evaluate $K_{E,A}$ from the slope of the adiabatic curves mentioned above, but corresponding to the point $q_s = \tilde{X}_s \approx 3.70$Å, and *not* to $q_s \approx 3.50$ Å. This leads to the values $K_E/\omega_s^E \approx 2.304$ and $K_A/\omega_s^A \approx 0.780$ used in Table 1.

Since the frequency of the stretching mode estimated previously both in the ground state ($\omega^X \simeq 140\ \text{cm}^{-1}$, cf. Ref. [4]) and in the excited state ($\omega_s^E = \omega_s^A \simeq 105\ \text{cm}^{-1}$, see above) does not differ too much from the value $\omega^E = \omega^A = 127\ \text{cm}^{-1}$ used earlier [17], we have performed a preliminary three-dimensional (3D) calculation by employing the same value for all frequencies $\omega^E = \omega^A = \omega_s^E = \omega_s^A = 127\ \text{cm}^{-1}$ (parameter set b in Tab. 1). These results are presented in the lower panel of Figure 3. The main difference with respect to the corresponding 2D results (upper panel of Fig. 3, parameter set a in Tab. 1) is the fact that this 3D-TPI spectrum is broader (by ∼20 nm) and blue shifted. The computed 3D spectrum remains regular, similar to the 2D spectrum; compare Figures 3a and 3b. In both spectra, the spacing between the lines with higher intensities is practically the same ($\sim$127 cm^{-1}). At variance to these, the experimental spectrum (see Fig. 2) of the B′ system is rather chaotic and the spacing between intense lines is roughly one third of the above value; compare Figure 2 with Figure 3. Even more significant that the discrepancies just mentioned is the fact that the wavelength ranges in Figures 2 and 3 are completely different. The theoretical spectrum (both for 2D and 3D calculations, see Figs. 3a and 3b) is located at significantly higher energies than the experimental one (Fig. 2).

Therefore, in the subsequent attempts we have abandoned the old values of ω^A, ω^E, λ, and f and optimized these parameters for the B′ system. Namely, we have looked for the best fit of the adiabatic potentials computed

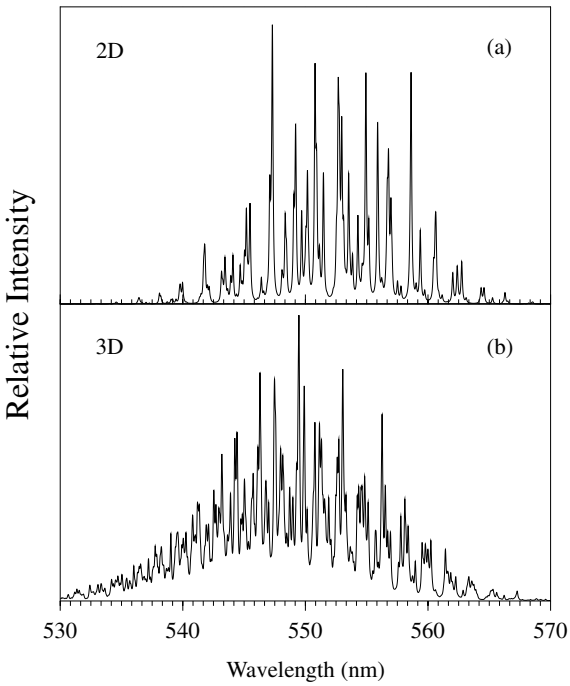

Fig. 4. Spectrum obtained by means of: (a) two-dimensional calculations using parameter set c, and (b) three-dimensional calculations using parameter set d. (For the parameter values, see Tab. 1.)

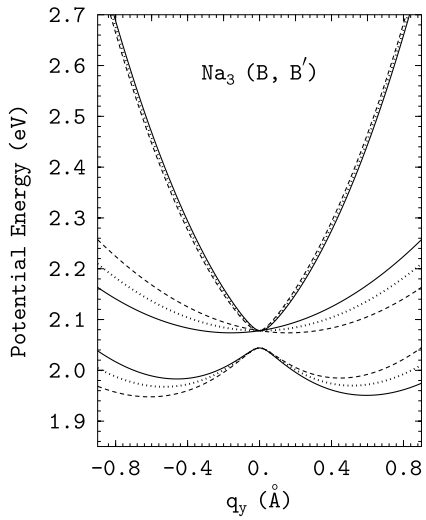

Fig. 5. Curves of the adiabatic potentials V_+, V_0, and V_- (from top to bottom) of equations (7, 8) without Jahn-Teller coupling ($k = 0$, $g = 0$; dotted lines, identical to the dashed lines of Fig. 1), plotted along with those obtained by including Jahn-Teller couplings (cf. Ref. [17]): $g = f/5.2$ and $k = \mp\lambda/5.2$ (solid and dashed lines for upper and lower signs, respectively). In all cases, the values of the pseudo-Jahn-Teller couplings are the same as in Figure 1.

ab initio (curves 4^2A_1, 3^2B_2 and 5^2A_1 in Fig. 4c of Ref. [4], shown as solid lines in Fig. 1) by using the analytic formulae (7) and (8) for V_-, V_0, and V_+, respectively. This fit, presented as dashed lines in Figure 1, yields significantly different values: $\omega^A = 127$ cm^{-1}, $\omega^E = 62$ cm^{-1}, and $\lambda/\omega^A = 1.85$ (note that, with the new ω^E, the value of the ratio $\lambda/\omega^E = 3.789$ is relatively close to the old value 3.07). Because the f-dependence of these adiabatic curves is insignificant, we have kept the old value for this parameter. Besides, we have accounted for a small difference between the values ϵ^E and ϵ^A (and set $\epsilon^E - \epsilon^A = 275$ cm^{-1}), as revealed by the ab initio calculations [4].

These new values have been used in all parameter sets of Table 1 starting with set c. So, parameter set c underlies the 2D calculation representing the best fit of available ab initio data [4] based on the PJT model. By augmenting parameter set c to fit ab initio data for the stretching mode, one arrives at parameter set d of Table 1. Therefore, the results of the 3D calculation relying upon parameter set d are the best one can obtain at present for the B′ system within a pure PJT model including all three vibrational modes of Na_3.

The results of the corresponding 2D and 3D calculations are presented in Figures 4a and 4b, respectively. By comparing the theoretical TPI spectra of Figure 4 and of Figure 4 with the spectrum recorded experimentally (Fig. 2) [21], one can see that the parameter values deduced by optimizing to the B′ system lead to a substantial improvement with respect to those derived earlier by optimized to the B system, in both 2D and 3D cases. Most significantly, the wavelength range of the theoretical spectrum (both for 2D and 3D cases) agrees very well with the spectrum recorded experimentally; compare Figures 4 and 2. Considerably more structure is visible in Figure 4b, the spectrum being significantly less regular than that of Figure 3b. This agrees qualitatively with the experimental spectrum, which displays the same feature. However, the details in the spectra of Figures 4b and 2 are too different and make a quantitative comparison impossible.

Above, we have disregarded possible JT couplings in the B′-excited state of Na_3. In fact, a simplified point charge model [25] has indicated that they are substantially smaller than the PJT couplings. Nevertheless, we have further performed 2D and 3D calculations by allowing for such small but nonvanishing JT terms $k = \pm\lambda/5.2$ and $g = f/5.2$, in accord with reference [25] (parameter sets e to h) [26]. These calculations demonstrate that, although small, the JT couplings may have a significant impact on the TPI spectrum.

An interesting effect obtained by using $k = +\lambda/5.2$ (parameter sets e and g) is that the spectra of the B and B′ systems become very close, a feature displayed by the experimental data [21]. This feature can be easily understood by inspecting the corresponding adiabatic potential energy curves in Figure 5. It is related to the location of the curves V_- and V_0, which determine the B spectrum and B′ spectrum, respectively. For positive values of Q_y and $k > 0$, the potential energy curves V_- and V_0 (dashed lines in Fig. 5) are closer than the dotted lines in the same figure, corresponding to $k = g = 0$. (Positive Q_y values are of interest since the ground state minimum is located at $q_y = +0.737$ Å.)

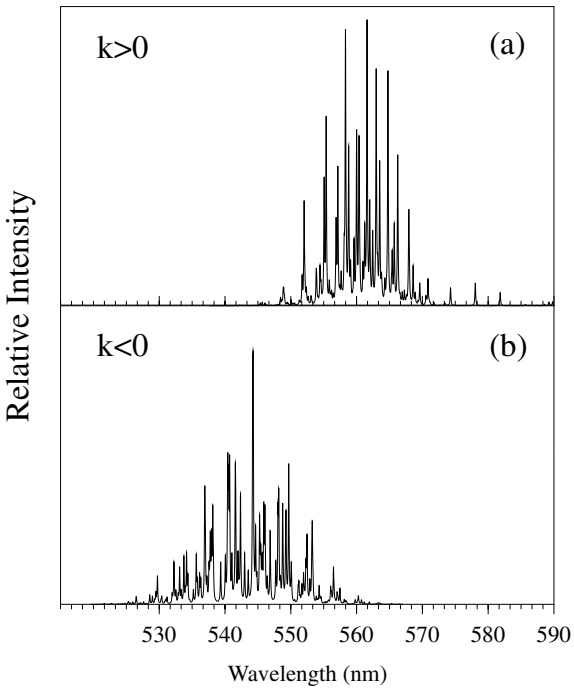

Fig. 6. Spectrum obtained by means of two-dimensional calculations accounting for both pseudo-Jahn-Teller and Jahn-Teller coupling terms using: (a) parameter set e, and (b) parameter set f. (For the parameter values, see Tab. 1.)

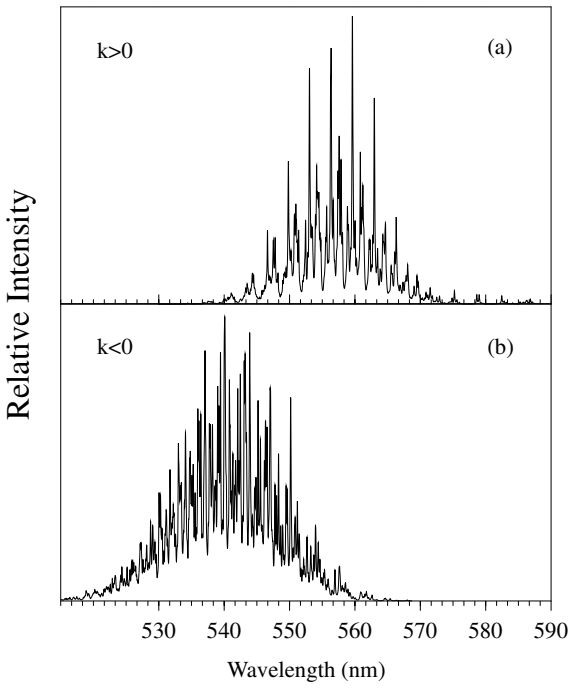

Fig. 7. Spectrum obtained by means of three-dimensional calculations accounting for both pseudo-Jahn-Teller and Jahn-Teller coupling terms using: (a) parameter set g, and (b) parameter set h. (For the parameter values, see Tab. 1.)

However, choosing a positive k-value one gets spectra exhibiting unambiguously less structure than seen experimentally; compare Figures 6a and 7a with Figure 2. On the other side, the spectra computed using a negative k-value (Figs. 6b and 7b) display richer structure. However, the weak point of this modelling is that the B- and B′-spectra become even more separated than for $k = g = 0$; that is, the B spectrum is further blue shifted with respect to Figure 4. Again, this behavior can be understand by inspecting the adiabatic curves for this case (solid lines in Fig. 5); indeed, the curves for V_- and V_0 become more distant from each other for $Q_y > 0$. Thus, the comparison between the spectra based on parameter sets c, e and g, or d, f, and h demonstrates not only the important part played by the JT couplings, but also the fact that the relative signs of the linear PJT and JT couplings have a significant influence on the calculated spectrum; this holds for both 2D and 3D cases.

Despite these open issues, let us emphasize the important implications of the present investigations for the nonadiabatic nuclear motion underlying the B′ system of Na_3. As pointed out above this is interpreted as arising from transitions to the middle of the three potential energy surfaces of Figures 1 and 5, which becomes degenerate with the upper surface for vanishing bending distortion (D_{3h} conformation, center of the figures). Moreover, owing to the additional totally symmetric mode, not included in the present figures, the E-A energy gap becomes modulated by the latter coordinate Q_s and also vanishes for a relevant displacement of the latter, beyond which the energetic ordering of the E and A states is reversed. The latter phenomenon amounts to a triple conical intersection. The nuclear motion at conical intersections is generally known to be highly nonadiabatic, i.e. proceeds on two (or more) potential energy surfaces simultaneously [27–29]. The same holds for degeneracies in general, such as those presented in Figures 1 and 5. The nuclear motion in the B′ system is thus subject to *multiple* nonadiabatic coupling effects. Other systems of this type have been addressed earlier in the literature [30–32]. However, what makes the B′ system unique is the presence of a Jahn-Teller distortion already in the initial state, i.e. the optical transition occurs for a finite value of the bending coordinate (of $q_y = 0.737$ Å, see above). This leads to higher final state vibronic energies and, thus, to an even richer variety of multi-state vibronic effects. The combination of initial-state and final-state vibronic effects represents an intriguing phenomenon which calls for further attention in future work.

4 Concluding remarks

In conclusion, in the present work on the nuclear dynamics of Na_3 we extended an earlier PJT approach to a higher-energy electronic state (B′ state). More coupling terms than before, and also the symmetric stretching mode have been included in this study, and all information available from existing ab initio data has been exhausted. Salient features of the experimental TPI spectrum of Na_3(B′) are also present in the calculated one, which allows us to

conclude on the importance of nonadiabatic interactions in this system. The particularly rich variety of (even multiple) nonadiabatic couplings has been emphasized. This once more underlines the unusual, and interesting, dynamical properties of electronically excited Na_3.

Nevertheless, the agreement between theory and experiment remains somewhat unsatisfactory. We believe that, in order to improve the understanding of the B′ state of Na_3, the theory should be extended in two directions. First, it is highly desirable to conduct more reliable ab initio studies. Second, dynamical calculations including more higher-order terms could also lead to theoretical spectra closer to those recorded experimentally. It is hoped that that these findings stimulate further, experimental and theoretical, work on this system.

This work has been supported financially by the Deutsche Forschungsgemeinschaft.

References

1. R.L. Martin, E.R. Davidson, Mol. Phys. **35**, 1713 (1978)
2. J.L. Martins, R. Car, J. Buttet, J. Chem. Phys. **78**, 5646 (1983)
3. M. Broyer, G. Delacrétaz, P. Labastie, J.-P. Wolf, L. Wöste, Phys. Rev. Lett. **57**, 1851 (1986)
4. F. Cocchini, T.H. Upton, W. Andreoni, J. Chem. Phys. **88**, 6068 (1988)
5. M. Broyer, G. Delacrétaz, G.-Q. Ni, R.L. Whetten, J.-P. Wolf, L. Wöste, Phys. Rev. Lett. **62**, 2100 (1989)
6. R. Meiswinkel, H. Köppel, Chem. Phys. **144**, 117 (1990)
7. Ph. Dugourd, J. Chevaleyre, J.P. Perrot, M. Broyer, J. Chem. Phys. **62**, 2332 (1990)
8. H.-A. Eckel, J.-M. Gress, W. Demtröder, J. Chem. Phys. **68**, 135 (1993)
9. T. Baumert, R. Thalweiser, G. Gerber, Chem. Phys. Lett. **209**, 29 (1993)
10. K. Kobe, H. Kühling, S. Rutz, E. Schreiber, J.P. Wolf, L. Wöste, Chem. Phys. Lett. **213**, 554 (1993)
11. A.J. Dobbyn, J. Hutson, J. Chem. Phys. **98**, 11428 (1994)
12. E. Schreiber, K. Kobe, A. Ruff, G. Sommer, L. Wöste, Chem. Phys. Lett. **242**, 106 (1995)
13. W.E. Ernst, S. Rakowsky, Phys. Rev. Lett. **74**, 58 (1995)
14. B. Reischl, R. de Vivie-Riedle, S. Rutz, E. Schreiber, J. Chem. Phys. **104**, 8857 (1996)
15. B. Kendrick, Phys. Rev. Lett. **79**, 2431 (1997)
16. H. von Busch, V. Dev, H.-A. Eckel, S. Kasahara, J. Wang, W. Demtröder, Phys. Rev. Lett. **81**, 4584 (1998)
17. R. Meiswinkel, H. Köppel, Z. Phys. D **19**, 63 (1991)
18. J. Schön, H. Köppel, Chem. Phys. Lett. **231**, 55 (1994)
19. J. Schön, H. Köppel, J. Phys. Chem. A **103**, 8579 (1999)
20. G. Delacrétaz, E.R. Grant, R.L. Whetten, L. Wöste, J.W. Zwanziger, Phys. Rev. Lett. **56**, 2598 (1986)
21. G. Delacrétaz, Ph.D. thesis, École Polytechnique Fédérale de Lausanne, Lausanne, Switzerland (1985)
22. R. de Vivie-Riedle, J. Gaus, V. Bonačić-Koutecký, J. Manz, B. Reischl-Lenz, P. Saalfrank, Chem. Phys. **223**, 1 (1997)
23. J. Gaus, K. Kobe, V. Bonačić-Koutecký, J. Manz, B. Reischl, S. Rutz, E. Schreiber, L. Wöste, J. Chem. Phys. **97**, 12509 (1993)
24. T.C. Thompson, D.G. Truhlar, C.A. Mead, Phys. Rev. Lett. **82**, 2392 (1985)
25. H. Köppel, R. Meiswinkel, Z. Phys. D **32**, 153 (1994)
26. One should note that the method of reference [25] does not permit to determine the relative signs of the JT and PJT couplings
27. H. Köppel, W. Domcke, L.S. Cederbaum, Adv. Chem. Phys. **57**, 59 (1984)
28. Chem. Phys. **259**, nos. 2-3, pp. 121-352 (special issue on *Conical Intersections in Photochemistry, Spectroscopy, and Chemical Dynamics*)
29. *Conical Intersections*, edited by W. Domcke, D.R. Yarkony, H. Köppel, Advanced Series in Physical Chemistry (World Scientific, Singapore, 2004), Vol. 15
30. M. Döscher, H. Köppel, Chem. Phys. **225**, 93 (1997)
31. S. Mahapatra, G.A. Worth, H.-D. Meyer, L.S. Cederbaum, H. Köppel, J. Phys. Chem. A **105**, 5567 (2001)
32. H. Köppel, M. Döscher, I. Bâldea, H.-D. Meyer, P.G. Szalay, J. Chem. Phys. **117**, 2657 (2002)